

# BSMamba: Brightness and Semantic Modeling for Long-Range Interaction in Low-Light Image Enhancement

Tongshun Zhang  
Jilin University

tszhang23@mails.jlu.edu.cn

Zijian Zhang  
Jilin University

zhangzijian@jlu.edu.cn

Pingping Liu\*  
Jilin University

liupp@jlu.edu.cn

Yubing Lu  
Jilin University

luyb24@mails.jlu.edu.cn

Mengen Cai  
Jilin University

caime24@mails.jlu.edu.cn

Qiuzhan Zhou  
Jilin University

zhouqz@jlu.edu.cn

## Abstract

Current low-light image enhancement (LLIE) methods face significant limitations in simultaneously improving brightness while preserving semantic consistency, fine details, and computational efficiency. With the emergence of state-space models, particularly Mamba, image restoration has achieved remarkable performance, yet existing visual Mamba approaches flatten 2D images into 1D token sequences using fixed scanning rules, critically limiting interactions between distant tokens with causal relationships and constraining their ability to capture meaningful long-range dependencies. To address these fundamental limitations, we propose BSMamba, a novel visual Mamba architecture comprising two specially designed components: Brightness Mamba and Semantic Mamba. The Brightness Mamba revolutionizes token interaction patterns by prioritizing connections between distant tokens with similar brightness levels, effectively addressing the challenge of brightness restoration in LLIE tasks through brightness-guided selective attention. Complementing this, the Semantic Mamba establishes priority interactions between tokens sharing similar semantic meanings, allowing the model to maintain contextual consistency by connecting semantically related regions across the image, thus preserving the hierarchical nature of image semantics during enhancement. By intelligently modeling tokens based on brightness and semantic similarity rather than arbitrary scanning patterns, BSMamba transcends the constraints of conventional token sequencing while adhering to the principles of causal modeling. Extensive experiments demonstrate that BSMamba achieves state-of-the-art performance in LLIE while preserving semantic consistency.

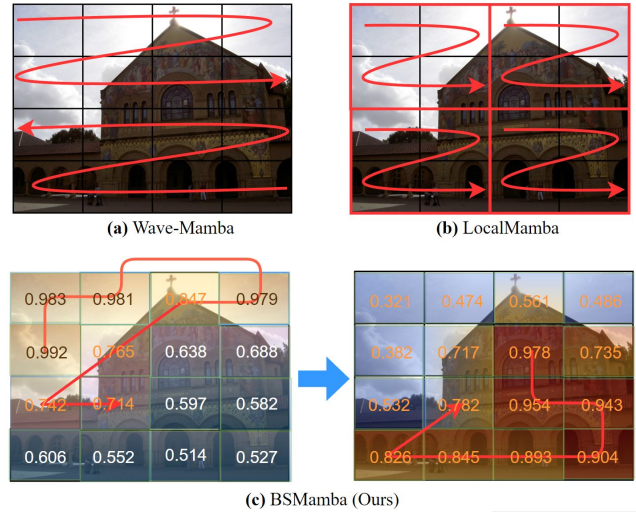


Figure 1. SS2D Scanning Strategies in State-Space Models. (a) The scanning structure of most visual Mamba models, such as Wave-Mamba, employs fixed horizontal, vertical, and reverse four-pass scanning strategies, which weaken interactions between causally related tokens. (b) The block-based scanning strategy, as in LocalMamba, also requires four scans within each block, lacking flexibility in interactions between causally related tokens. (c) Our BSMamba adopts a dual-layer scanning strategy based on brightness hierarchy scores and semantic hierarchy scores, allowing flexible interactions between causally related tokens while reducing scanning complexity.

## 1. Introduction

Images captured in low-light conditions often suffer from low contrast, color distortion, detail loss, and even complete information loss. LLIE aims to restore brightness and visual content in such images. Its advancements have significantly expanded its applications in fields like autonomous driving, security surveillance, and multimedia [7, 16, 25, 33].

Traditional LLIE methods, including histogram equal-

\*Corresponding author

ization [23], gamma correction [19], and Retinex-based approaches [26, 47], typically struggle with extreme lighting conditions due to generalization issues, often neglecting noise and detail degradation, resulting in unsatisfactory performance. Deep learning-based LLIE methods [2, 43, 45, 56] attempt to learn the mapping between low-light and normal-light images through neural networks, demonstrating performance and visual quality superior to traditional approaches. However, most deep learning-based LLIE methods [18, 35, 46, 50] overlook brightness consistency, color fidelity, and fine image details during enhancement, leading to unpleasant color distortion, detail loss, and suboptimal brightness. Additionally, constrained by parameter efficiency, many LLIE methods [24, 43, 45, 52] cannot maintain both high performance and computational efficiency.

Recently, state-space models [9] have developed rapidly as alternatives to CNNs and Transformers, offering significant advantages in long sequence modeling while reducing computational complexity from quadratic to linear. Visual Mamba-based methods [13, 21, 41, 54] have demonstrated superior performance over dominant Transformer models across various vision tasks, including image segmentation, super-resolution, and LLIE. However, applying Mamba to the visual domain still faces two critical limitations:

First, while causal relationships between tokens in language naturally align with state-space model scanning mechanisms, in 2D images, tokens with causal relationships may be spatially distant, weakening the modeling capabilities between causally related tokens and limiting long-range modeling and generalization [12, 44]. Furthermore, flattening images into sequences disrupts the spatial dependencies and local adjacencies inherent in 2D images. This fundamental difference between language and vision domains creates challenges for adapting Mamba to visual tasks.

Second, current visual Mamba-based LLIE methods [1, 41, 55] generally flatten 2D images into 1D sequences using fixed scanning rules, as illustrated in Fig. 1(a) for WaveMamba [55]. To compensate for interactions between adjacent and distant tokens, these methods often employ multi-directional forward and reverse scanning strategies. However, MambaIR [12, 13] has demonstrated that such multi-directional scanning contains significant information redundancy and fails to mitigate the decay of interactions between distant tokens. Various visual Mamba [20, 31] approaches have attempted to address this by dividing images into multiple windows or clusters (Fig. 1(b)), with each processed separately to ensure causally related tokens are handled together. Nevertheless, these approaches still lack flexibility in handling various object scales, and the problem of long-range decay between causally related tokens remains unresolved.

To address these limitations, we introduce BSMamba,

a novel Mamba architecture for LLIE tasks. BSMamba comprises Brightness Mamba and Semantic Mamba components. Brightness Mamba models the brightness essence of LLIE tasks by treating brightness levels as causal attributes between pixels, encouraging preferential interactions between spatially distant pixels with similar brightness properties, thereby enhancing long-range brightness-based causal interactions. Semantic Mamba leverages instance segmentation results to generate attention maps. Unlike conventional attention mechanisms that treat all regions equally, Semantic Mamba dynamically assigns attention scores based on segmentation confidence scores while maintaining the relative importance of features within each instance. Semantic Mamba unfolds the image into a 1D sequence according to each object’s attention score, encouraging priority interactions between distant tokens with similar semantic scores on a semantically consistent basis. Brightness Mamba and Semantic Mamba in BSMamba require only two scanning passes, improving efficiency while effectively enhancing brightness and semantic interactions between distant tokens, as shown in Fig. 1(c). After processing by BSMamba, the predicted image is finally fed into a Detail Enhancement Network (DE-Net) to further optimize image edge details. The overall framework follows a three-step strategy: ensuring brightness, semantic, and detail consistency throughout the LLIE process.

Overall, our contributions are summarized as follows:

- We propose the BSMamba framework, which simultaneously focuses on brightness restoration, semantic consistency, and detail enhancement in LLIE tasks.
- Brightness Mamba models long-range brightness causal interactions by prioritizing connections between spatially distant pixels with similar brightness levels, effectively enhancing brightness restoration.
- Semantic Mamba establishes long-range semantic causal interactions by dynamically assigning attention scores based on instance segmentation, ensuring semantically consistent enhancement across distant regions.
- BSMamba achieves state-of-the-art (SOTA) performance in LLIE tasks with improved efficiency and superior restoration of brightness, semantics, and details.

## 2. Related Work

### 2.1. Low-Light Scene Enhancement

Traditional LLIE methods, such as histogram equalization [23], gamma correction [19], and Retinex theory [26], often introduce artifacts and noise under extreme or complex lighting conditions. With the rise of deep learning, neural network-based LLIE methods [45, 46, 48] have become dominant. Retinex-based approaches [8, 42], like Retinexformer [2], combine Retinex theory with Transformers to address long-range dependencies, while IAGC [38] intro-

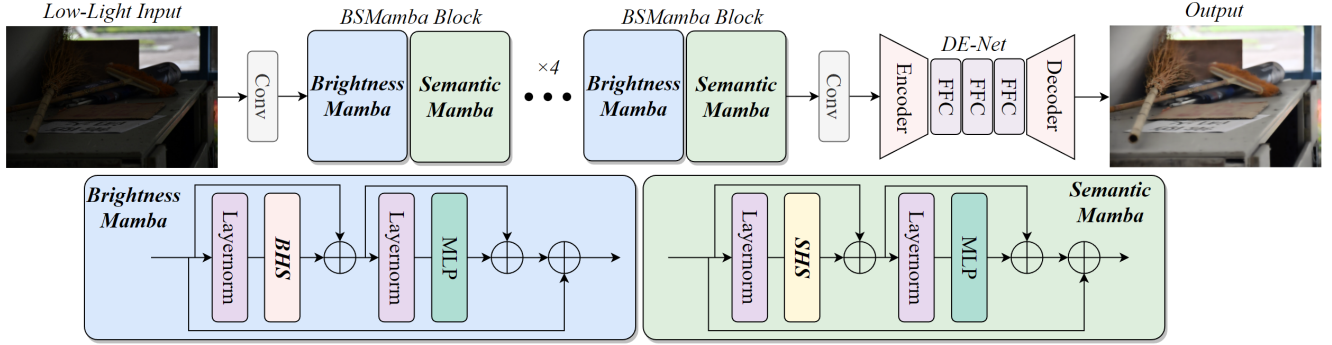


Figure 2. Overall Structure of BSMamba. BSMamba consists of four BSMamba blocks and the DE-Net.

duces learnable gamma correction for adaptive enhancement. In addition, many methods incorporate priors to guide LLIE. For instance, SMG-LLE [46] uses structural maps for enhancement, SKF [43] integrates semantic priors, and LEDN [40] incorporates depth information for improved restoration. However, these methods face challenges such as errors from pre-trained models and increased computational costs due to prior generation modules. Recently, frequency-domain LLIE methods have emerged. FourLLIE [35] enhances brightness via amplitude mapping in Fourier space, while DMFourLLIE [50] jointly enhances phase and amplitude using infrared modalities and brightness attention. WaveMamba [55] applies state-space models in the wavelet domain for brightness enhancement and noise removal, and WalMaFa [34] combines wavelet-based Mamba with Fourier adjustments. However, these methods rely on vanilla Mamba and fail to address its limitations in modeling long-range interactions in 2D images.

## 2.2. State-Space Models

State-space models (SSMs) have gained attention for addressing long-range dependencies, as demonstrated by LSSL [11] and S4 [10], which serve as alternatives to CNNs and Transformers. Mamba [9], a selective SSM, has been extended to visual tasks like classification [54], restoration [5, 13], and fusion [27]. In LLIE, RetinexMamba [1] combines Retinexformer with SSMs for faster processing, while WaveMamba [55] and WalMaFa [34] leverage Mamba for low-frequency feature extraction and global brightness modeling. However, these methods rely on vanilla Mamba, which struggles with weakened long-range interactions in 2D images. To address this, improved methods have been proposed. LocalMamba [20] uses window-based scanning for better local detail representation, QuadMamba [44] employs quadtree-based scanning to preserve spatial locality, and ARM clusters adjacent blocks for efficient scanning. LLEMamba [51] adopts bidirectional scanning to balance local and global focus. However, these approaches fail to model causal relationships be-

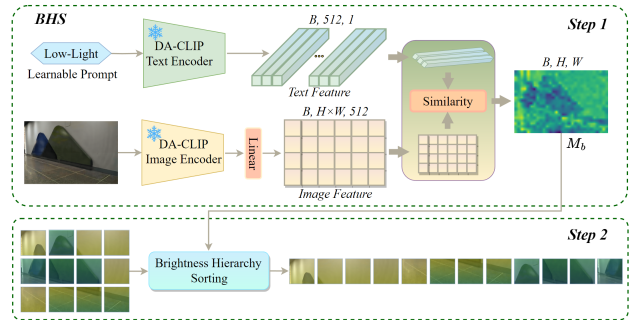


Figure 3. Brightness Hierarchy Scanning (BHS) in Brightness Mamba. The BHS structure enables brightness-aware token interactions by prioritizing tokens with similar brightness levels, regardless of their spatial positions.

tween pixels, limiting effective interactions and overall performance.

## 3. Method

### 3.1. Overview

The proposed BSMamba framework is designed to address the challenges of LLIE by simultaneously modeling brightness and semantic consistency. As illustrated in Fig. 2, the input low-light image is first processed through an initial convolutional layer to extract features. These feature maps are then refined by a series of BSMamba blocks, where the Brightness Mamba and Semantic Mamba modules enhance the interactions between causally related tokens based on brightness and semantic hierarchies. The refined feature maps are subsequently passed through a Detail Enhancement Network (DE-Net) to reconstruct spatial details, producing the final enhanced image. Below, we provide a detailed description of each component.

### 3.2. Brightness Mamba

To overcome the fundamental limitations of existing visual Mamba methods in modeling long-range dependencies, we

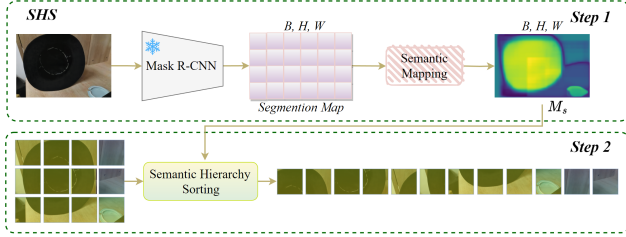


Figure 4. Semantic Hierarchy Scanning (SHS) in Semantic Mamba. The SHS structure facilitates semantic-aware token interactions by grouping tokens based on their semantic significance, ensuring consistent enhancement within object instances.

propose Brightness Mamba [9, 55], a novel component that prioritizes interactions between distant tokens with similar brightness levels. Specifically, Brightness Mamba utilizes DA-CLIP [30] to compute brightness grading scores by calculating similarity scores between all image pixels and brightness descriptors, reflecting the brightness levels of all pixels across the image. We unfold the image into a 1D sequence based on brightness scores, where pixels with similar brightness levels are grouped together, promoting effective interaction between spatially distant pixels with similar brightness characteristics.

This approach specifically targets the core requirements of LLIE tasks by enabling more effective brightness-guided enhancement across the image. As shown in Fig. 2, the proposed Brightness Mamba module integrates the Brightness Hierarchy Scanning (BHS) mechanism into the state-space structure:

$$\mathbf{X}' = \mathbf{X} + \text{BHS}(\text{LayerNorm}(\mathbf{X})), \quad (1)$$

$$\mathbf{Y} = \mathbf{X}' + \text{MLP}(\text{LayerNorm}(\mathbf{X}')), \quad (2)$$

where  $\mathbf{X}$  is the input image. The BHS mechanism, as shown in Fig. 3, consists of two key steps: 1) brightness hierarchy computation using DA-CLIP [30], and 2) brightness hierarchy sorting.

**Step 1: Brightness Hierarchy Computation.** Traditional visual Mamba methods scan images using fixed patterns, which fail to capture meaningful causal relationships between distant pixels. In LLIE tasks, pixels with similar brightness properties often require similar enhancement operations, regardless of their spatial distance. DA-CLIP predicts high-quality feature embeddings from degraded low-light images. Therefore, we leverage a pre-trained DA-CLIP model to compute brightness similarity scores, enabling brightness-aware token interactions:

$$\mathbf{M}_b = \text{Sim}(\Phi_{\text{image}}(\mathbf{X}), \Phi_{\text{text}}(\text{'low-light'})), \quad (3)$$

where  $\Phi_{\text{image}}$  extracts image features from the DA-CLIP image encoder, followed by projection to align feature di-

mensions and normalization for cosine similarity computation.  $\Phi_{\text{text}}$  encodes the text descriptor 'low-light.' The resulting similarity map quantifies the alignment of each pixel with the concept of 'low-light,' effectively creating a brightness hierarchy map  $\mathbf{M}_b \in \mathbb{R}^{B \times H \times W}$  across the image.

**Step 2: Brightness Hierarchy Sorting.** Based on the brightness hierarchy map  $\mathbf{M}_b$  generated in Step 1, we perform Brightness Hierarchy Sorting to reorder the image tokens according to their brightness levels:

$$\hat{\mathbf{X}}_{\text{sort}}, \hat{\mathbf{I}}_{\text{sort}} = \text{Sort}(\mathbf{M}_b, \mathbf{X}), \quad (4)$$

where  $\hat{\mathbf{X}}_{\text{sort}}$  represents the 1D sequence of tokens reordered based on their brightness scores, ensuring that pixels with similar brightness characteristics are processed sequentially, regardless of their spatial positions in the original image.  $\hat{\mathbf{I}}_{\text{sort}}$  is the inverse index used to reorder the tokens back to their original positions. As shown in Fig. 3, tokens from different spatial locations but with similar brightness levels (indicated by blocks of similar colors) are grouped together in the sorted sequence. By prioritizing interactions between tokens with similar brightness levels, Brightness Mamba effectively models the causal relationships of brightness across the image space, addressing the core challenges of LLIE.

### 3.3. Semantic Mamba

While addressing brightness consistency is crucial for LLIE tasks, maintaining semantic coherence between object instances is equally essential to ensure perceptually natural results. To accomplish this, we propose the Semantic Mamba module, as shown in Fig. 2, which leverages instance segmentation information to guide token interactions based on semantic relationships.

Similar to Brightness Mamba, Semantic Mamba incorporates the SHS mechanism within a state-space block structure. As shown in Fig. 4, the Semantic Hierarchy Scanning (SHS) mechanism consists of two key steps: (1) semantic mapping using Mask R-CNN [17], and (2) semantic hierarchy sorting.

**Step 1: Semantic Mapping.** To effectively capture semantic information from low-light images, we utilize a pre-trained Mask R-CNN model to generate instance segmentation masks. Unlike traditional scanning patterns that fail to respect semantic boundaries, our approach identifies object instances and assigns attention scores based on their semantic significance:

$$\mathbf{M}_s = \mathcal{M}_{\text{semantic}}(G_{\text{Mask-RCNN}}(\mathbf{X})), \quad (5)$$

where  $\mathbf{X}$  is the input image,  $G_{\text{Mask-RCNN}}$  generates instance segmentation masks with confidence scores, and  $\mathcal{M}_{\text{semantic}}$  maps these instances to a continuous semantic attention map  $\mathbf{M}_s \in \mathbb{R}^{B \times H \times W}$ .

Methods	LSRW-Nikon			#Param (M)	#FLOPs (G)
	PSNR $\uparrow$	SSIM $\uparrow$	LPIPS $\downarrow$		
MIRNet [48]	17.10	0.5022	0.2170	31.79	785.1
Kind++ [53]	14.79	0.4749	0.2111	8.27	-
SGM [47]	15.73	0.4971	0.2234	2.31	-
FECNet [18]	17.06	0.4999	0.2192	0.15	5.82
HDMNet [28]	16.65	0.4870	0.2157	2.32	-
FourLLIE [35]	17.82	0.5036	0.2150	0.12	4.07
UHDFour [24]	17.94	0.5195	0.2546	17.54	4.78
Retinexformer [2]	17.64	0.5082	0.2784	1.61	15.57
WaveMamba [55]	17.34	0.5192	0.2294	1.26	7.22
DMFourLLIE [50]	17.04	0.5294	0.2178	0.75	5.81
RetinexMamba [1]	17.59	0.5133	0.2534	3.59	34.76
Ours	<b>18.04</b>	<b>0.5327</b>	<b>0.2012</b>	0.68	8.15

Table 1. Quantitative comparison on LSRW-Nikon dataset. The best results are highlighted in bold.

The semantic mapping function  $\mathcal{M}_{\text{semantic}}$  implements a dynamic grading strategy:

$$\mathcal{M}_{\text{semantic}}(\mathbf{I}) = \sum_{i=1}^n \mathbf{M}_i \cdot \mathbf{S}_i \cdot \mathcal{G}_i + \mathbf{M}_{\text{bg}} \cdot \mathcal{G}_{\text{bg}}, \quad (6)$$

where  $\mathbf{I}$  represents the segmentation results,  $n$  is the number of detected instances,  $\mathbf{M}_i$  and  $\mathbf{S}_i$  are the mask and confidence score for the  $i$ -th instance,  $\mathcal{G}_i$  is the grading function that maps the  $i$ -th instance to a specific attention range,  $\mathbf{M}_{\text{bg}}$  is the background mask, and  $\mathcal{G}_{\text{bg}}$  maps the background to the lowest attention range. Specifically, we define  $n + 1$  hierarchical ranges (including the background) as:

$$\mathcal{G}_i = \left[ \frac{i}{n+1}, \frac{i+1}{n+1} \right], i \in \{0, 1, \dots, n\}, \quad (7)$$

where  $i = 0$  corresponds to the background. This dynamic grading ensures that: 1) Each detected instance is assigned a unique attention range, with higher confidence instances receiving higher attention values. 2) The background regions receive the lowest attention values. 3) Different parts within the same instance maintain their relative importance.

**Step 2: Semantic Hierarchy Sorting.** Based on the semantic attention map  $\mathbf{M}_s$  generated in Step 1, we perform Semantic Hierarchy Sorting to reorder image tokens according to their semantic significance:

$$\tilde{\mathbf{X}}_{\text{sort}}, \tilde{\mathbf{I}}_{\text{sort}} = \text{Sort}(\mathbf{M}_s, \mathbf{X}), \quad (8)$$

similar to the BHS, where  $\tilde{\mathbf{X}}_{\text{sort}}$  represents the tokens reordered based on their semantic scores, ensuring that tokens from the same semantic entity are processed together regardless of their spatial locations.  $\tilde{\mathbf{I}}_{\text{sort}}$  contains the indices to reorder tokens back to their original positions. As illustrated in Fig. 4, tokens with similar semantic significance (represented by similar colors) are grouped together in the

Methods	LSRW-Huawei			#Param (M)	#FLOPs (G)
	PSNR $\uparrow$	SSIM $\uparrow$	LPIPS $\downarrow$		
NPE [37]	17.08	0.3905	0.2303	-	-
LIME [14]	17.00	0.3816	0.2069	-	-
SRIE [8]	13.42	0.4282	0.2166	-	-
Kind [52]	16.58	0.5690	0.2259	8.02	34.99
MIRNet [48]	19.98	0.6085	0.2154	31.79	785.1
Kind++ [53]	15.43	0.5695	0.2366	8.27	-
SGM [47]	18.85	0.5991	0.2492	2.31	-
FECNet [18]	21.09	0.6119	0.2341	0.15	5.82
HDMNet [28]	20.81	0.6071	0.2375	2.32	-
SNR-Aware [45]	20.67	0.5911	0.1923	39.12	26.35
FourLLIE [35]	21.11	0.6256	0.1825	0.12	4.07
UHDFour [24]	19.39	0.6006	0.2466	17.54	4.78
Retinexformer [2]	21.23	0.6309	0.1699	1.61	15.57
WaveMamba [55]	21.19	0.6391	0.1818	1.26	7.22
UHDFormer [36]	20.64	0.6244	0.1812	0.34	3.24
DMFourLLIE [50]	21.47	0.6331	0.1781	0.75	5.81
RetinexMamba [1]	20.88	0.6298	0.1689	3.59	34.76
Ours	<b>21.49</b>	<b>0.6435</b>	<b>0.1613</b>	0.68	8.15

Table 2. Quantitative comparison on LSRW-Huawei dataset. The best results are highlighted in bold.

Methods	LOL-v1			LOL-v2-Real		
	PSNR $\uparrow$	SSIM $\uparrow$	LPIPS $\downarrow$	PSNR $\uparrow$	SSIM $\uparrow$	LPIPS $\downarrow$
FourLLIE [35]	20.99	0.8071	0.0952	23.45	0.8450	0.0613
UHDFour [24]	22.89	0.8147	0.0934	27.27	0.8579	0.0617
SNR-SKF [43]	20.51	0.7110	0.1810	21.82	0.7468	0.1513
Retinexformer [2]	22.71	0.8177	0.0922	24.55	0.8434	0.0627
RetinexMamba [1]	23.15	0.8210	0.0876	27.31	0.8667	0.0551
WaveMamba [55]	22.76	0.8419	0.0791	27.87	0.8935	0.0451
DMFourLLIE [50]	21.58	0.8349	0.0821	26.74	0.8792	0.0528
Ours	<b>24.07</b>	<b>0.8521</b>	<b>0.0709</b>	<b>29.07</b>	<b>0.9013</b>	<b>0.0401</b>

Table 3. Quantitative comparison on LOL dataset. The best results are highlighted in bold.

sorted sequence. This approach ensures that: 1) Pixels belonging to the same object instance are processed sequentially. 2) Tokens with similar semantic roles can interact effectively regardless of their spatial distance.

The Semantic Mamba module complements the Brightness Mamba module within the BSMamba framework. While Brightness Mamba focuses on enhancing the brightness consistency of the image based on illumination-related features, Semantic Mamba ensures that the semantic relationships between different image regions are preserved during enhancement. This dual-perspective approach addresses both critical aspects of LLIE: Brightness Mamba establishes long-range dependencies between pixels with similar illumination conditions. Semantic Mamba maintains semantic coherence by ensuring consistent enhancement within object instances.



Figure 5. Visual comparison on LSRW-Nikon dataset. Zoomed-in provide a clearer comparison.

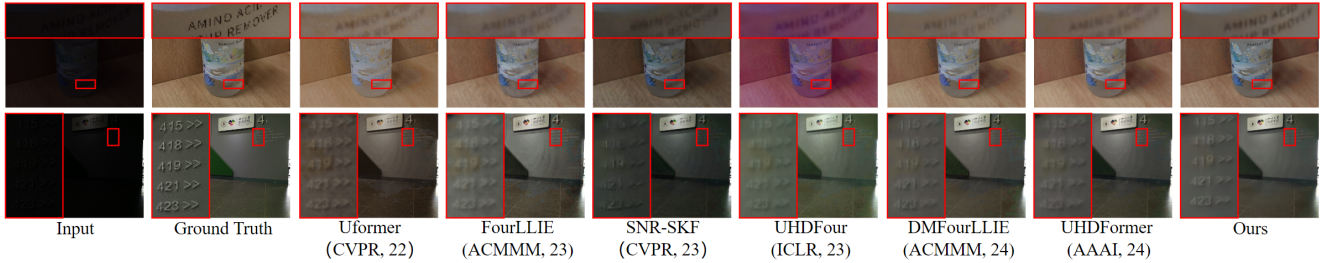


Figure 6. Visual comparison on LSRW-Huawei dataset. Zoomed-in provide a clearer comparison.

### 3.4. Detail Enhancement Network (DE-Net)

After processing with BSMamba blocks, which restore brightness relationships and semantic consistency, we further refine the spatial details and texture information through our proposed Detail Enhancement Network (DE-Net). As illustrated in Fig. 2, DE-Net is specifically designed to enhance fine-grained details that may remain partially degraded after the initial enhancement. The DE-Net adopts an encoder-decoder architecture with Fast Fourier Convolution (FFC) [3] blocks in the bottleneck. The FFC architecture divides feature channels into spatial and spectral branches, allowing the network to simultaneously capture local spatial details and global frequency patterns, which is particularly beneficial for enhancing texture and structural details [6].

To further enhance the structural integrity of the reconstructed images, we incorporate edge guidance through a specialized Canny edge loss:

$$\mathcal{L}_{\text{canny}} = \text{BCE}(\mathcal{E}(\mathbf{Y}), \mathcal{E}(\mathbf{Y}_{\text{gt}})), \quad (9)$$

where  $\mathcal{E}$  represents the Canny edge extraction operation,  $\mathbf{Y}$  is the predicted enhanced image,  $\mathbf{Y}_{\text{gt}}$  is the ground truth image, and BCE denotes the binary cross-entropy loss function [32].

The overall optimization objective is:

$$\mathcal{L}_{\text{total}} = \lambda_1 \mathcal{L}_1 + \lambda_2 \mathcal{L}_{\text{ssim}} + \lambda_3 \mathcal{L}_{\text{canny}} \quad (10)$$

where loss weights  $\lambda_1, \lambda_2, \lambda_3 = [1.0, 0.5, 0.1]$ ,  $\mathcal{L}_1$  is the  $l_1$  loss,  $\mathcal{L}_{\text{ssim}}$  denotes the structural similarity (SSIM)

loss [39].

## 4. Experiments

### 4.1. Datasets and Experimental Setting

Our method is evaluated on four widely recognized datasets for LLIE: LOL [47], LOLv2-Real [47], LSRW-Huawei [15], LSRW-Nikon [15]. The LOL dataset comprises 485 paired images for training and 15 pairs for testing, with LOLv2-Real [47] used for evaluation. The LSRW-Huawei dataset, captured with a Huawei P40 Pro, includes 3,150 training pairs and 20 test pairs, while the LSRW-Nikon dataset, collected using the Nikon D7500, contains 2,450 training pairs and 30 test pairs. Additionally, we evaluate on two unpaired datasets: DICM [22] (64 images) and NPE [37] (85 images).

The model is implemented and trained end-to-end using the PyTorch framework. During training, images are randomly cropped to  $256 \times 256$  pixels and augmented with random horizontal and vertical flips. We optimize the model using the ADAM optimizer, starting with a learning rate of  $4.0 \times 10^{-4}$ , and employ a multi-step learning rate scheduler. The batch size is set to 8, and the training process spans  $1.5 \times 10^5$  iterations. All experiments are conducted on two NVIDIA 4090 GPUs.

### 4.2. Overall Performance

We compare our approach against a variety of state-of-the-art LLIE methods, including traditional algorithms (LIME [14], NPE [37], SRIE [8]), deep learning-based techniques (Kind [52], Kind++ [53], MIRNet [48],

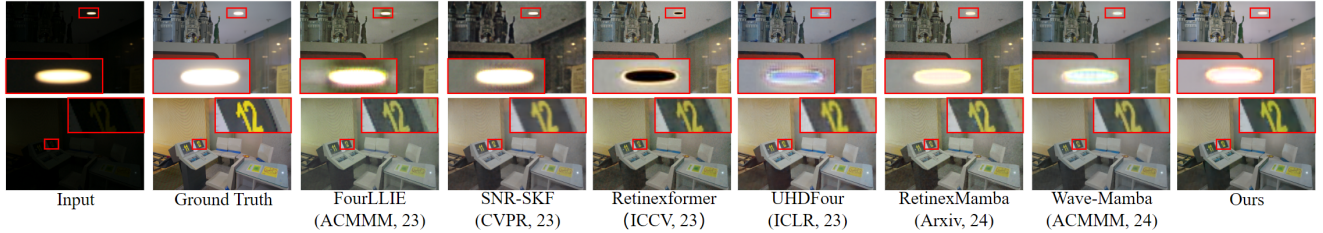


Figure 7. Visual comparison on LOL dataset. Zoomed-in provide a clearer comparison.

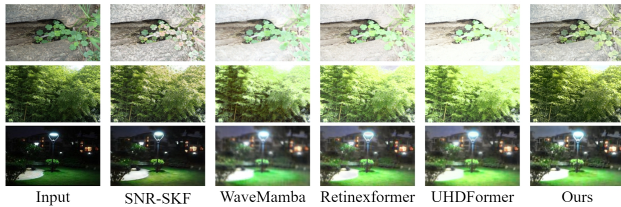


Figure 8. Visual comparison on DICM (first and second rows) and NPE (third row) datasets. Zoomed-in provide a clearer comparison.

Configurations	PSNR $\uparrow$	SSIM $\uparrow$	LPIPS $\downarrow$
w/o Brightness Mamba	21.03	0.6357	0.1893
w/o Semantic Mamba	21.14	0.6374	0.1795
w/o DE-Net	20.94	0.6389	0.1747
BSMamba Block $\rightarrow$ Vanilla SS2D	20.57	0.6351	0.1905
Brightness Mamba + Semantic Mamba	20.57	0.6351	0.1905
Brightness Mamba C Semantic Mamba	20.57	0.6351	0.1905
Semantic Mamba $\leftrightarrow$ Brightness Mamba	21.34	0.6421	0.1682
DA-CLIP $\rightarrow$ Brightness Histogram	21.36	0.6402	0.1665
DA-CLIP $\rightarrow$ Y component	21.23	0.6384	0.1714
Ours	<b>21.49</b>	<b>0.6435</b>	<b>0.1613</b>

Table 4. Ablation studies and experimental configurations.

SGM [47], HDMNet [28], SNR-Aware [45], SNR-SKF [43], Retinexformer [2], UHDFormer [36]), Fourier-based models (FourLLIE [35], FECNet [18], UHD-Four [24], DMFourLLIE [50]), and Mamba-based approaches (RetinexMamba [1], Wave-Mamba [55], MambaIR [13]). For fair evaluation, all deep learning models are trained on the same datasets using their respective publicly available implementations.

We adopt Peak Signal-to-Noise Ratio (PSNR), Structural Similarity Index (SSIM) [39], and Learned Perceptual Image Patch Similarity (LPIPS) [49] as evaluation metrics. Higher PSNR and SSIM values, along with lower LPIPS scores, indicate better visual quality and closer resemblance to the ground truth.

**Quantitative Results on LOL, LOLv2-Real, LSRW-Huawei and LSRW-Nikon.** 1) Tab. 1 reports the quantitative results on the LSRW-Nikon dataset, where our method achieves the best PSNR, SSIM, and LPIPS scores, signifi-

cantly outperforming existing approaches. Compared to methods like RetinexMamba, our approach not only ensures a lightweight design but also substantially reduces computational overhead. 2) Tab. 2 presents results on the LSRW-Huawei dataset, where our method also achieves state-of-the-art (SOTA) performance, excelling in brightness restoration, structural preservation, and perceptual quality. Notably, compared to lightweight models such as UHDFormer and DMFourLLIE, our approach consistently delivers superior performance, highlighting its robustness and efficiency. 3) Tab. 3 shows the comparison results on the LOL-v1 and LOLv2-Real datasets. Our method achieves the highest PSNR, SSIM, and LPIPS scores, outperforming all competing methods.

**Qualitative Comparison.** To intuitively demonstrate restoration quality, we provide visual comparisons with state-of-the-art methods. 1) Fig. 5 shows visual results on the LSRW-Nikon dataset. In local regions, existing methods exhibit noticeable blurring and color distortion, particularly in areas with fine textures. For example, methods like MambaIR and UHDFour fail to recover details and introduce artifacts. In contrast, our approach preserves color and luminance fidelity while maintaining clear texture structures, achieving high consistency with the Ground Truth. 2) Fig. 6 presents visual comparisons on the LSRW-Huawei dataset. For challenging local regions, our method outperforms others in restoring text details and object textures. Additionally, the color distribution is more natural, particularly in difficult areas. 3) Fig. 7 illustrates visual comparisons on the LOL dataset. In the first row, other methods misinterpret bright light sources, causing noticeable color shifts. In contrast, our approach preserves the true brightness of light sources while effectively enhancing darker areas, ensuring natural luminance balance and mitigating artifacts that degrade visual quality.

**Qualitative Comparison on DICM and NPE Datasets.** As shown in Fig. 8, our method delivers superior visual results. In the first two rows, methods like UHDFormer and WaveMamba suffer from overexposure in brighter regions, while SNR-SKF introduces noticeable color distortions. In the third row, other methods cause significant texture blurring, whereas our approach preserves fine textures, enhances color fidelity, and improves illumination contrast.

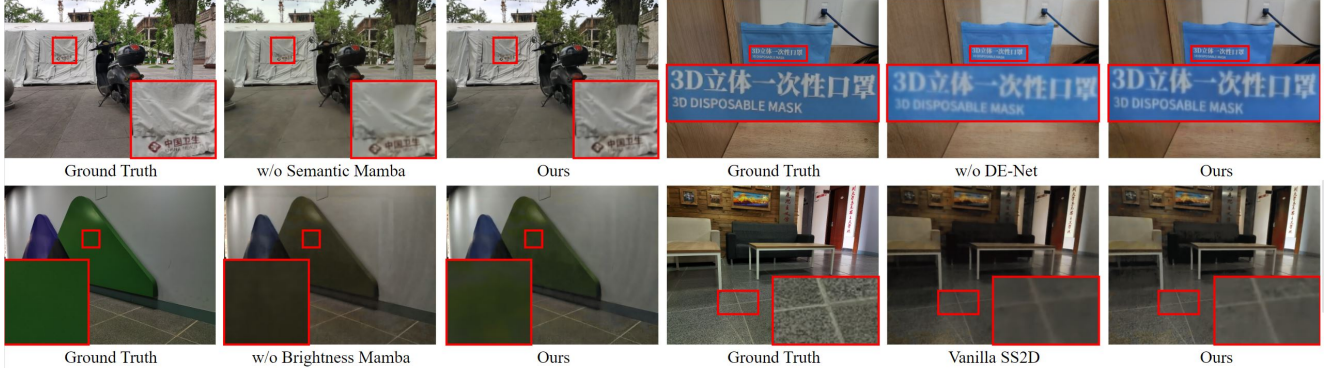


Figure 9. Visualization of Ablation Studies.

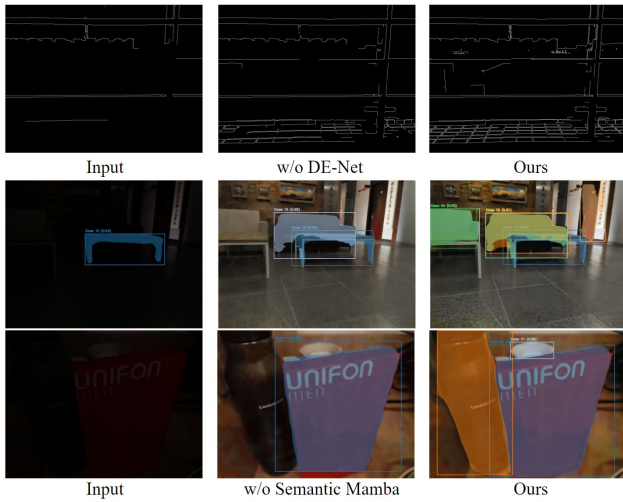


Figure 10. Validation on Downstream Applications. We validate DE-Net’s effectiveness through edge detection, which is sensitive to image details, and Semantic Mamba’s effectiveness through instance segmentation. Observations show that our full model achieves the best performance in both edge detection and instance segmentation.

Additionally, our method demonstrates greater robustness and adaptability across diverse lighting conditions.

### 4.3. Ablation Study and Experimental Configurations

We conduct ablation experiments to validate the independent contributions of each module in our framework. As shown in Fig.9, **w/o** represents the removal of specific modules: **w/o Brightness Mamba** significantly reduces brightness enhancement; **w/o Semantic Mamba** degrades semantic consistency and instance-level performance; **w/o DE-Net** results in blurred details and reduced edge sharpness. **BSMamba Block**  $\rightarrow$  **Vanilla SS2D** replaces our Brightness and Semantic Mamba scanning strategies with a vanilla

state-space 2D (SS2D) approach, causing severe degradation in both brightness and image details.

The performance of different configurations is presented in Tab.4. We evaluate the structural design of the Brightness Mamba and Semantic Mamba components: **Brightness Mamba + Semantic Mamba** modifies them to operate in parallel with summed outputs; **Brightness Mamba C Semantic Mamba** concatenates their outputs; **Semantic Mamba  $\leftrightarrow$  Brightness Mamba** swaps their order. We also assess the impact of different brightness scoring mechanisms in the Brightness Mamba module: **DA-CLIP**  $\rightarrow$  **Brightness Histogram** replaces DA-CLIP with a brightness histogram, calculated by normalizing pixel intensity distributions and using histogram bins as brightness scores; **DA-CLIP**  $\rightarrow$  **Y component** uses the Y component from the YCrCb color space as the brightness score. Our full model, integrating all components and using DA-CLIP for brightness scoring, achieves the best performance, as shown in the last row.

### 4.4. Downstream Applications

Beyond the brightness-focused Brightness Mamba, we introduce Semantic Mamba and DE-Net to enhance semantic consistency and detail restoration. To validate their effectiveness, we evaluate our method on downstream tasks, including instance segmentation (Mask R-CNN [17] pre-trained on COCO dataset [29]) and edge detection [4], which assess semantic preservation and detail recovery, respectively. Fig.9 illustrates the results of removing the corresponding modules and compares them. The visual comparisons further confirm the performance gains achieved by incorporating Semantic Mamba and DE-Net.

## 5. Conclusion

In this paper, we propose BSMamba, a novel visual Mamba architecture designed to overcome the fundamental limitations of existing LLIE methods. By introducing the Brightness Mamba and Semantic Mamba, our approach redefines

the label interaction paradigm based on brightness and semantic similarity, enabling effective long-range modeling of causally related labels while maintaining spatial and contextual consistency. Furthermore, BSMamba provides new insights and inspiration for future research. In the future, we plan to explore more generalized scanning strategies for brightness and semantic Mamba, or develop task-specific customized scanning strategies tailored to specific downstream tasks, aiming to guide and enhance the performance of related tasks.

## References

- [1] Jiesong Bai, Yuhao Yin, and Qiyuan He. Retinexmamba: Retinex-based mamba for low-light image enhancement. *arXiv preprint arXiv:2405.03349*, 2024. 2, 3, 5, 7
- [2] Yuanhao Cai, Hao Bian, Jing Lin, Haoqian Wang, Radu Timofte, and Yulun Zhang. Retinexformer: One-stage retinex-based transformer for low-light image enhancement. In *ICCV*, 2023. 2, 5, 7
- [3] Lu Chi, Borui Jiang, and Yadong Mu. Fast fourier convolution. *Advances in Neural Information Processing Systems*, 33:4479–4488, 2020. 6
- [4] Lijun Ding and Ardeshtir Goshtasby. On the canny edge detector. *Pattern recognition*, 34(3):721–725, 2001. 8
- [5] Chenyu Dong, Chen Zhao, Weiling Cai, and Bo Yang. Omamba: O-shape state-space model for underwater image enhancement. *arXiv preprint arXiv:2408.12816*, 2024. 3
- [6] Qiaole Dong, Chenjie Cao, and Yanwei Fu. Incremental transformer structure enhanced image inpainting with masking positional encoding. In *CVPR*, pages 11358–11368, 2022. 6
- [7] Zhipeng Du, Miaojing Shi, and Jiankang Deng. Boosting object detection with zero-shot day-night domain adaptation. In *ICCV*, pages 12666–12676, 2024. 1
- [8] Xueyang Fu, Delu Zeng, Yue Huang, Xiao-Ping Zhang, and Xinghao Ding. A weighted variational model for simultaneous reflectance and illumination estimation. In *CVPR*, pages 2782–2790, 2016. 2, 5, 6
- [9] Albert Gu and Tri Dao. Mamba: Linear-time sequence modeling with selective state spaces. *arXiv preprint arXiv:2312.00752*, 2023. 2, 3, 4
- [10] Albert Gu, Karan Goel, and Christopher Ré. Efficiently modeling long sequences with structured state spaces. *arXiv preprint arXiv:2111.00396*, 2021. 3
- [11] Albert Gu, Isys Johnson, Karan Goel, Khaled Saab, Tri Dao, Atri Rudra, and Christopher Ré. Combining recurrent, convolutional, and continuous-time models with linear state space layers. *Advances in neural information processing systems*, 34:572–585, 2021. 3
- [12] Hang Guo, Yong Guo, Yaohua Zha, Yulun Zhang, Wenbo Li, Tao Dai, Shu-Tao Xia, and Yawei Li. Mambairv2: Attentive state space restoration. *arXiv preprint arXiv:2411.15269*, 2024. 2
- [13] Hang Guo, Jinmin Li, Tao Dai, Zhihao Ouyang, Xudong Ren, and Shu-Tao Xia. Mambair: A simple baseline for image restoration with state-space model. In *ECCV*, pages 222–241. Springer, 2025. 2, 3, 7
- [14] Xiaojie Guo, Yu Li, and Haibin Ling. Lime: Low-light image enhancement via illumination map estimation. *IEEE TIP*, 26(2):982–993, 2016. 5, 6
- [15] Jiang Hai, Zhu Xuan, Ren Yang, Yutong Hao, Fengzhu Zou, Fang Lin, and Songchen Han. R2rnet: Low-light image enhancement via real-low to real-normal network. *Journal of Visual Communication and Image Representation*, 90: 103712, 2023. 6
- [16] Khurram Azeem Hashmi, Goutham Kallempudi, Didier Stricker, and Muhammad Zeshan Afzal. Featenhancer: Enhancing hierarchical features for object detection and beyond under low-light vision. In *CVPR*, pages 6725–6735, 2023. 1
- [17] Kaiming He, Georgia Gkioxari, Piotr Dollár, and Ross Girshick. Mask r-cnn. In *ICCV*, pages 2961–2969, 2017. 4, 8
- [18] Jie Huang, Yajing Liu, Feng Zhao, Keyu Yan, Jinghao Zhang, Yukun Huang, Man Zhou, and Zhiwei Xiong. Deep fourier-based exposure correction network with spatial-frequency interaction. In *ECCV*, pages 163–180. Springer, 2022. 2, 5, 7
- [19] Shih-Chia Huang, Fan-Chieh Cheng, and Yi-Sheng Chiu. Efficient contrast enhancement using adaptive gamma correction with weighting distribution. *IEEE TIP*, 22(3):1032–1041, 2012. 2
- [20] Tao Huang, Xiaohuan Pei, Shan You, Fei Wang, Chen Qian, and Chang Xu. Localmamba: Visual state space model with windowed selective scan. *arXiv preprint arXiv:2403.09338*, 2024. 2, 3
- [21] Yongsong Huang, Tomo Miyazaki, Xiaofeng Liu, and Shinichiro Omachi. Irsrmamba: Infrared image super-resolution via mamba-based wavelet transform feature modulation model. *arXiv preprint arXiv:2405.09873*, 2024. 2
- [22] Chulwoo Lee, Chul Lee, and Chang-Su Kim. Contrast enhancement based on layered difference representation. In *ICIP*, pages 965–968. IEEE, 2012. 6
- [23] Chulwoo Lee, Chul Lee, and Chang-Su Kim. Contrast enhancement based on layered difference representation of 2d histograms. *IEEE TIP*, 22(12):5372–5384, 2013. 2
- [24] Chongyi Li, Chun-Le Guo, Man Zhou, Zhexin Liang, Shangchen Zhou, Ruicheng Feng, and Chen Change Loy. Embeddingfourier for ultra-high-definition low-light image enhancement. In *ICLR*, 2023. 2, 5, 7
- [25] Jinlong Li, Baolu Li, Zhengzhong Tu, Xinyu Liu, Qing Guo, Felix Juefei-Xu, Runsheng Xu, and Hongkai Yu. Light the night: A multi-condition diffusion framework for unpaired low-light enhancement in autonomous driving. In *ICCV*, pages 15205–15215, 2024. 1
- [26] Mading Li, Jiaying Liu, Wenhan Yang, Xiaoyan Sun, and Zongming Guo. Structure-revealing low-light image enhancement via robust retinex model. *IEEE TIP*, 27(6):2828–2841, 2018. 2
- [27] Zhe Li, Haiwei Pan, Kejia Zhang, Yuhua Wang, and Fengming Yu. Mambadfuse: A mamba-based dual-phase model for multi-modality image fusion. *arXiv preprint arXiv:2404.08406*, 2024. 3

- [28] Yudong Liang, Bin Wang, Wenqi Ren, Jiaying Liu, Wenjian Wang, and Wangmeng Zuo. Learning hierarchical dynamics with spatial adjacency for image enhancement. In *ACM MM*, pages 2767–2776, 2022. [5](#), [7](#)
- [29] Tsung-Yi Lin, Michael Maire, Serge Belongie, James Hays, Pietro Perona, Deva Ramanan, Piotr Dollár, and C Lawrence Zitnick. Microsoft coco: Common objects in context. In *Computer vision–ECCV 2014: 13th European conference, zurich, Switzerland, September 6–12, 2014, proceedings, part v 13*, pages 740–755. Springer, 2014. [8](#)
- [30] Ziwei Luo, Fredrik K Gustafsson, Zheng Zhao, Jens Sjölund, and Thomas B Schön. Controlling vision-language models for universal image restoration. *arXiv preprint arXiv:2310.01018*, 3(8), 2023. [4](#)
- [31] Sucheng Ren, Xianhang Li, Haoqin Tu, Feng Wang, Fangxun Shu, Lei Zhang, Jieru Mei, Linjie Yang, Peng Wang, Heng Wang, et al. Autoregressive pretraining with mamba in vision. *arXiv preprint arXiv:2406.07537*, 2024. [2](#)
- [32] Usha Ruby, Vamsidhar Yendapalli, et al. Binary cross entropy with deep learning technique for image classification. *Int. J. Adv. Trends Comput. Sci. Eng.*, 9(10), 2020. [6](#)
- [33] Tao Sun, Mattia Segu, Janis Postels, Yuxuan Wang, Luc Van Gool, Bernt Schiele, Federico Tombari, and Fisher Yu. Shift: a synthetic driving dataset for continuous multi-task domain adaptation. In *CVPR*, pages 21371–21382, 2022. [1](#)
- [34] Junhao Tan, Songwen Pei, Wei Qin, Bo Fu, Ximing Li, and Libo Huang. Wavelet-based mamba with fourier adjustment for low-light image enhancement. In *Proceedings of the Asian Conference on Computer Vision*, pages 3449–3464, 2024. [3](#)
- [35] Chenxi Wang, Hongjun Wu, and Jin Zhi. Fourllie: Boosting low-light image enhancement by fourier frequency information. In *ACM MM*, 2023. [2](#), [3](#), [5](#), [7](#)
- [36] Cong Wang, Jinshan Pan, Wei Wang, Gang Fu, Siyuan Liang, Mengzhu Wang, Xiao-Ming Wu, and Jun Liu. Correlation matching transformation transformers for uhd image restoration. In *AAAI*, pages 5336–5344, 2024. [5](#), [7](#)
- [37] Shuhang Wang, Jin Zheng, Hai-Miao Hu, and Bo Li. Naturalness preserved enhancement algorithm for non-uniform illumination images. *IEEE TIP*, 22(9):3538–3548, 2013. [5](#), [6](#)
- [38] Yinglong Wang, Zhen Liu, Jianzhuang Liu, Songcen Xu, and Shuaicheng Liu. Low-light image enhancement with illumination-aware gamma correction and complete image modelling network. In *ICCV*, pages 13128–13137, 2023. [2](#)
- [39] Zhou Wang, Alan C Bovik, Hamid R Sheikh, and Eero P Simoncelli. Image quality assessment: from error visibility to structural similarity. *IEEE TIP*, 13(4):600–612, 2004. [6](#), [7](#)
- [40] Zhen Wang, Dongyuan Li, Guang Li, Ziqing Zhang, and Renhe Jiang. Multimodal low-light image enhancement with depth information. In *ACM MM*, pages 4976–4985, 2024. [3](#)
- [41] Jiangwei Weng, Zhiqiang Yan, Ying Tai, Jianjun Qian, Jian Yang, and Jun Li. Mamballie: Implicit retinex-aware low light enhancement with global-then-local state space. *Advances in Neural Information Processing Systems*, 37:27440–27462, 2025. [2](#)
- [42] Wenhui Wu, Jian Weng, Pingping Zhang, Xu Wang, Wenhao Yang, and Jianmin Jiang. Uretinex-net: Retinex-based deep unfolding network for low-light image enhancement. In *CVPR*, pages 5901–5910, 2022. [2](#)
- [43] Yuhui Wu, Chen Pan, Guoqing Wang, Yang Yang, Jiwei Wei, Chongyi Li, and Heng Tao Shen. Learning semantic-aware knowledge guidance for low-light image enhancement. In *CVPR*, pages 1662–1671, 2023. [2](#), [3](#), [5](#), [7](#)
- [44] Fei Xie, Weijia Zhang, Zhongdao Wang, and Chao Ma. Quadmamba: Learning quadtree-based selective scan for visual state space model. *Advances in Neural Information Processing Systems*, 37:117682–117707, 2025. [2](#), [3](#)
- [45] Xiaogang Xu, Ruixing Wang, Chi-Wing Fu, and Jiaya Jia. Snr-aware low-light image enhancement. In *CVPR*, pages 17714–17724, 2022. [2](#), [5](#), [7](#)
- [46] Xiaogang Xu, Ruixing Wang, and Jiangbo Lu. Low-light image enhancement via structure modeling and guidance. In *CVPR*, pages 9893–9903, 2023. [2](#), [3](#)
- [47] Wenhao Yang, Wenjing Wang, Haofeng Huang, Shiqi Wang, and Jiaying Liu. Sparse gradient regularized deep retinex network for robust low-light image enhancement. *IEEE TIP*, 30:2072–2086, 2021. [2](#), [5](#), [6](#), [7](#)
- [48] Syed Waqas Zamir, Aditya Arora, Salman Khan, Munawar Hayat, Fahad Shahbaz Khan, Ming-Hsuan Yang, and Ling Shao. Learning enriched features for real image restoration and enhancement. In *ECCV*, pages 492–511. Springer, 2020. [2](#), [5](#), [6](#)
- [49] Richard Zhang, Phillip Isola, Alexei A Efros, Eli Shechtman, and Oliver Wang. The unreasonable effectiveness of deep features as a perceptual metric. In *CVPR*, pages 586–595, 2018. [7](#)
- [50] Tongshun Zhang, Pingping Liu, Ming Zhao, and Haotian Lv. Dmfourllie: Dual-stage and multi-branch fourier network for low-light image enhancement. In *ACM MM*, pages 7434–7443, 2024. [2](#), [3](#), [5](#), [7](#)
- [51] Xuanqi Zhang, Haijin Zeng, Jinwang Pan, Qiangqiang Shen, and Yongyong Chen. Llemamba: Low-light enhancement via relighting-guided mamba with deep unfolding network. *arXiv preprint arXiv:2406.01028*, 2024. [3](#)
- [52] Yonghua Zhang, Jiawan Zhang, and Xiaojie Guo. Kindling the darkness: A practical low-light image enhancer. In *ACM MM*, pages 1632–1640, 2019. [2](#), [5](#), [6](#)
- [53] Yonghua Zhang, Xiaojie Guo, Jiayi Ma, Wei Liu, and Jiawan Zhang. Beyond brightening low-light images. *IJCV*, 129:1013–1037, 2021. [5](#), [6](#)
- [54] Lianghui Zhu, Bencheng Liao, Qian Zhang, Xinlong Wang, Wenyu Liu, and Xinggang Wang. Vision mamba: Efficient visual representation learning with bidirectional state space model. *arXiv preprint arXiv:2401.09417*, 2024. [2](#), [3](#)
- [55] Wenbin Zou, Hongxia Gao, Weipeng Yang, and Tongtong Liu. Wave-mamba: Wavelet state space model for ultra-high-definition low-light image enhancement. In *ACM MM*, pages 1534–1543, 2024. [2](#), [3](#), [4](#), [5](#), [7](#)
- [56] Wenbin Zou, Hongxia Gao, Tian Ye, Liang Chen, Weipeng Yang, Shasha Huang, Hongsheng Chen, and Sixiang Chen. Vqcnir: Clearer night image restoration with vector-quantized codebook. In *AAAI*, pages 7873–7881, 2024. [2](#)